

Article

Optimization and Engineering of a Self-Sufficient CYP102 Enzyme from *Bacillus amyloliquefaciens* towards Synthesis of In-Chain Hydroxy Fatty Acids

Li Zong^{1,2}, Yan Zhang², Zhengkang Shao¹, Yingwu Wang¹, Zheng Guo² , Renjun Gao^{1,*} 
and Bekir Engin Eser^{2,*}

¹ Key Laboratory for Molecular Enzymology and Engineering, The Ministry of Education, School of Life Science, Jilin University, Changchun 130021, China; zongli18@mails.jlu.edu.cn (L.Z.); shaozk18@mails.jlu.edu.cn (Z.S.); wyw@jlu.edu.cn (Y.W.)

² Department of Biological and Chemical Engineering, Faculty of Technical Sciences, Aarhus University, Gustav Wieds Vej 10, 8000 Aarhus, Denmark; yanzhang@bce.au.dk (Y.Z.); guo@bce.au.dk (Z.G.)

* Correspondence: gaorj@jlu.edu.cn (R.G.); bekireser@bce.au.dk (B.E.E.)

Abstract: Cytochrome P450 (CYP) mediated enzymatic hydroxylation of fatty acids present a green alternative to chemical synthesis of hydroxy fatty acids (HFAs), which are high-value oleochemicals with various uses in materials industry and medical field. Although many CYPs require the presence of additional reductase proteins for catalytic activity, self-sufficient CYPs have their reductase partner naturally fused into their catalytic domain, leading to a greatly simplified biotransformation process. A recently discovered self-sufficient CYP, BAMF2522 from *Bacillus amyloliquefaciens* DSM 7, exhibits novel regioselectivity by hydroxylating in-chain positions of palmitic acid generating ω -1 to ω -7 HFAs, a rare regiodiversity profile among CYPs. Besides, F89I mutant of BAMF2522 expanded hydroxylation up to ω -9 position of palmitic acid. Here, we further characterize this enzyme by determining optimum temperature and pH as well as thermal stability. Moreover, using extensive site-directed and site-saturation mutagenesis, we obtained BAMF2522 variants that demonstrate greatly increased regioselectivity for in-chain positions (ω -4 to ω -9) of various medium to long chain fatty acids. Remarkably, when a six-residue mutant was reacted with palmitic acid, 84% of total product content was the sum of ω -7, ω -8 and ω -9 HFA products, the highest in-chain selectivity observed to date with a self-sufficient CYP. In short, our study demonstrates the potential of a recently identified CYP and its mutants for green and sustainable production of a variety of in-chain hydroxy enriched HFAs.



Citation: Zong, L.; Zhang, Y.; Shao, Z.; Wang, Y.; Guo, Z.; Gao, R.; Eser, B.E. Optimization and Engineering of a Self-Sufficient CYP102 Enzyme from *Bacillus amyloliquefaciens* towards Synthesis of In-Chain Hydroxy Fatty Acids. *Catalysts* **2021**, *11*, 665. <https://doi.org/10.3390/catal11060665>

Academic Editor: Maria H. L. Ribeiro

Received: 3 April 2021

Accepted: 21 May 2021

Published: 23 May 2021

Keywords: Cytochrome P450; self-sufficient enzyme; hydroxy fatty acid; regioselectivity; protein engineering; *Bacillus amyloliquefaciens*

Publisher's Note: MDPI stays neutral with regard to jurisdictional claims in published maps and institutional affiliations.



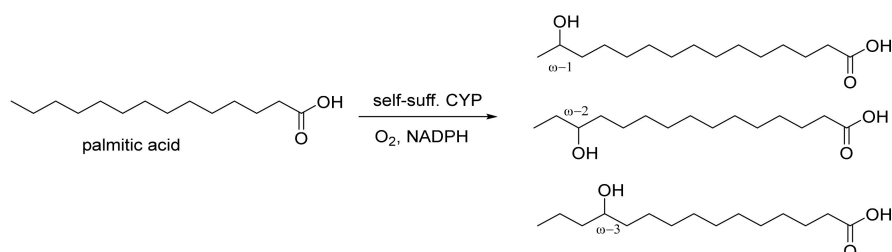
Copyright: © 2021 by the authors. Licensee MDPI, Basel, Switzerland. This article is an open access article distributed under the terms and conditions of the Creative Commons Attribution (CC BY) license (<https://creativecommons.org/licenses/by/4.0/>).

1. Introduction

Cytochrome P450 enzymes (CYPs) are a ubiquitous superfamily of heme-dependent monooxygenases that carry out chemically difficult biotransformations on various substrates (e.g., fatty acids) [1,2]. CYPs catalyze a wide range of chemical reactions including hydroxylation [3], decarboxylation [4], epoxidation [5], reductive dehalogenation [6], dealkylation [7], sulfoxidation [8], and anti-Markovnikov oxidation [9]. The typical reaction of CYPs is regio- and stereoselective insertion of one of the oxygen atoms from molecular oxygen into an organic substrate (hydroxylation), where the other oxygen atom is reduced to the level of water [10]. CYP102A1 (BM3) from *Bacillus megaterium* is the most extensively studied CYP to date for practical applications as well as for mechanistic and structural studies [3,11]. Whereas most CYPs require separate reductase protein partners for the transfer of electrons from NAD(P)H into the catalytic heme center, BM3 is a natural fusion protein, where catalytic heme domain and the electron supplying reductase domain

are present together as a single-polypeptide. This self-sufficient electronic delivery system [12–14], along with high expression levels in heterologous hosts and efficient turnover numbers [3,15,16], make BM3 ideal for biotechnology applications. In addition to BM3, there are other self-sufficient CYPs (CYP102, CYP116 and CYP505 families), many of which have been characterized only in the last decade [11,17].

One of the most common type of conversions performed by many of the CYPs, especially self-sufficient enzymes, is the hydroxylation of medium to long-chain fatty acids to produce hydroxy fatty acids (HFAs) [11,18] (Scheme 1). HFAs are value-added chemicals that can be used in the manufacturing of a broad range of materials including cosmetics, adhesives, plasticizers, bioplastics, lubricants, surfactants, viscosity modifiers and coatings [19–22]. Ricinoleic acid (12-hydroxy-9-*cis*-octadecenoic acid) and 12-hydroxystearic acid are the most common HFAs used in industry [23]. The fatty acid chain length and position of the hydroxy group dictate the physicochemical properties of a HFA, thus its application area and potential [22]. Moreover, HFAs and their derivatives have been shown to have various beneficial medical effects including antibiotic, anti-diabetic, anti-inflammatory and anti-cancer activities. HFAs, as metabolites of human gut microbiome, were proposed to play a role in the regulation of host energy metabolism [24]. Fatty acid esters of HFAs (FAHFAs) are naturally occurring bioactive lipids that exhibit anti-diabetic and anti-inflammatory effects [25–28]. Over 25 families of FAHFAs were identified in humans differing by composition of their fatty acids and the position of the ester bond between HFA and fatty acid [26]. Another group of medically important HFAs are specialized proresolving mediators (SPMs), such as lipoxins and resolvins (di-, tri- or poly-hydroxy derivatives of C20 and C22 polyunsaturated fatty acids), which play important roles in resolution of inflammation, stimulation of tissue regeneration and tumor growth suppression [29–31]. Accordingly, regio- and stereoselective synthesis of HFAs is desired for accessing medically useful HFAs and their derivatives.



Scheme 1. Representative reaction of self-sufficient CYPs with palmitic acid, demonstrating most common HFA products. NADPH; nicotinamide adenine dinucleotide phosphate.

Selective hydroxylation of unactivated C-H bonds in a long hydrocarbon backbone, like the one on a fatty acid chain, is quite challenging by chemical means [13,32]. In this regard, enzymatic synthesis of HFAs by CYPs, especially self-sufficient families, present a green and sustainable method for production of these high-value oleochemicals and their derivatives [11,17,23]. However, there are challenges that prevent practical utilization of CYPs for HFA synthesis, such as low activity levels and low operational stability of the enzyme [11]. For example, CYP substrates are often poorly soluble in water, making high reaction temperatures and presence of organic co-solvents among desired process conditions. Thus, information on optimum temperature and pH as well as on stability is quite important for the design of efficient biocatalytic processes with CYPs [33,34]. Moreover, most fatty acid oxidizing CYPs carry out their hydroxylation reaction on sub-terminal positions (positions next to the omega end; mainly ω -1, ω -2 and ω -3; Scheme 1). There are only a few among all CYPs, some engineered and recently discovered enzymes, which preferably generate in-chain (ω -4 to ω -9) hydroxylated HFAs [18,35–37]. Such middle chain hydroxylated HFAs are useful for production of lactones in fragrance industry, as material additives and as precursors for medically useful compounds, such as FAHFAs [22,23,37]. Overall, hydroxy groups on different positions of the fatty acid chain gives varying molec-

ular properties to HFA molecule, which can be advantageous for certain industrial and medical applications.

In an earlier study, we identified two self-sufficient CYP102 family members from the bacterium *Bacillus amyloliquefaciens* DSM 7 [36]. One of these enzymes, BAMF2522, prefers in-chain hydroxylation with seven hydroxylation products from ω -1 to ω -7 HFAs observed, a rare property among CYPs studied to date. Moreover, a single mutant variant (F89I) further shifted hydroxylation up to ω -9 position for palmitic acid (hexadecanoic acid; C16:0) [36]. In this study, we determined the optimum pH and temperature conditions of BAMF2522, as well as its thermostability. Furthermore, the enzyme was engineered by site-directed mutagenesis at single and multiple sites and by site saturation mutagenesis at single sites to modulate its regioselectivity. Resulting mutants were tested towards various medium to long-chain fatty acids. Some mutants exhibited significantly increased preference for in-chain positions, with over 90% selectivity for the formation of ω -4 to ω -9 products in certain cases.

2. Results and Discussion

2.1. Temperature, pH and Thermostability Analysis

Optimum temperature and pH of BAMF2522 were determined using purified enzyme preparations. Active protein concentration was based on heme content (Figure S1). Temperature dependence was evaluated within a range of 10–70 °C. pH dependence experiments were performed using various buffers from pH 5.0 to pH 10.5. In order to account for the possible additional effects from the type of buffer salt, activity at pH range 6.5–8.0 was measured with at least two different buffer systems of the same pH. In all assays, activities were determined by measuring hydroxylation of pentadecanoic acid (C15:0), towards which the enzyme has the highest activity. Our results demonstrated that optimal temperature and pH conditions of BAMF2522 were 30 °C and pH 7.0 (HEPES buffer), respectively (Figure 1). The activity levels of the enzyme from 20 °C to 50 °C were at least 60% of the maximum activity at 30 °C. Here, we should also emphasize that the effect of temperature, especially at lower temperature values, may not be due only to the increase in rate constants according to Arrhenius equation, but also due to increased solubility of the fatty acid substrate, leading to fluctuations in activity. Interestingly, the enzyme retained about 50% of its optimal activity level when assayed at 60 °C for 15 min (Figure 1a). To our knowledge, such high relative activity levels at 60 °C were not observed with wild-type or engineered full-length BM3 enzymes [38]. In terms of pH, moderate to high activity levels (about 40% or more of the optimal activity) were observed within a pH range of 6.5–8.5, similar to BM3 and its fungal orthologue CYP505A30 [39–41]. However, a strong dependence on the type of the buffer salt has also been observed. Although HEPES buffer gave the highest measured activity levels at a single pH, assays in sodium phosphate and Tris-HCl buffers had reasonably high activities over a moderate pH range of 6.5–8.0 and 7.1–8.5, respectively (Figure 1b). Notably, there was a steep decline in activity between pH 6.0 and 6.5 as well as between pH 8 and pH 9.

In order to investigate thermostability of BAMF2522, purified enzyme was incubated at various temperatures from 4 °C to 70 °C for 1 hour. This was immediately followed by measurement of the residual enzyme activity at 30 °C for 20 min with a shaking speed of 400 rpm. BAMF2522 was stable from 4 °C to 40 °C, exhibiting almost same level of conversion at this temperature range (Figure 2). Yet, the enzyme activity was totally lost at 50 °C and further. When considered together with the temperature dependence analysis described above (Figure 1a), it is apparent that the enzyme can retain much of its activity at 50 °C and 60 °C for a short assay period of 15 min; however one hour pre-incubation at respective temperatures was sufficient to totally abolish the activity. Thus, in order to get more insight into thermostability of the enzyme at high temperatures, we performed incubations for various time points from 15 min to 90 min at 60 °C. After 15 min incubation at 60 °C, 40% of the activity was retained, whereas the activity was completely lost after 30 min incubation (Figure S2). This result is consistent with the high relative activities

observed at 50 °C and 60 °C in 15 min temperature dependence assays (Figure 1a). There are a few literature studies in literature on thermostability of BM3 [38,42,43]. Although it is difficult to make direct comparison for BAMF2522 with those studies due to different conditions used, one study clearly shows that full-length wild-type BM3 loses its activity completely following 10 min incubation period at 55 °C [43]. Thus, BAMF2522 has a better thermostability compared to BM3 and will be a good starting point for further stabilization attempts through engineering.

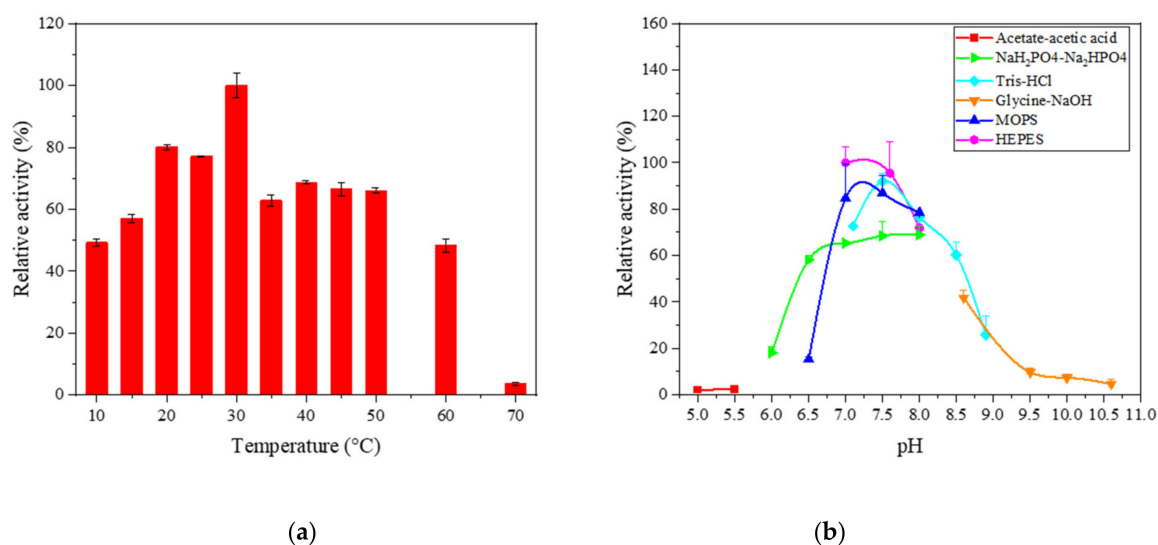


Figure 1. Temperature (a) and pH dependence (b) profiles for the hydroxylation activity by BAMF2522. All results were expressed as means \pm SD of at least two separate experiments (numerical data with errors are given in Tables S2 and S3). In temperature dependence experiments (a), reactions contained (in 0.5 mL total volume) 0.6 mM substrate (C15:0), 4.0 μ M enzyme, 0.2 mM NADPH (nicotinamide adenine dinucleotide phosphate) and 5% ethanol. Assays were carried out at varying temperatures for 15 min, with a shaking speed of 500 rpm in 50 mM Tris-HCl, pH 7.5 buffer. The activity value at 30 °C was defined as 100%. In the case of pH dependence experiments, after pre-incubation with different buffers, the reactions were carried out at 30 °C for 15 min at 500 rpm shaking speed. Reactions contained (in 0.5 mL) 1 mM substrate (C15:0), 4.0 μ M enzyme, 0.2 mM NADPH and 5% ethanol. The activity value at HEPES (4-(2-hydroxyethyl)-1-piperazineethanesulfonic acid), pH 7.0 was defined as 100%. MOPS; (3-(N-morpholino)propanesulfonic acid).

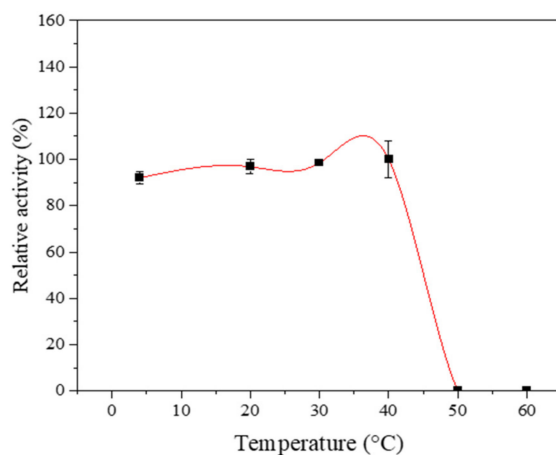


Figure 2. Thermostability analysis of BAMF2522. The enzyme (1.2 μ M) was preincubated for 60 min at the indicated temperatures (4 °C, 20 °C, 30 °C, 40 °C, 50 °C, 60 °C and 70 °C) before measuring the residual enzyme activity at 30 °C for a period of 20 min with 400 rpm shaking. No activity was observed at 50 °C, 60 °C and 70 °C. The assays were carried out in 50 mM Tris-HCl, pH 7.5 and 5% ethanol, with 0.6 mM of C15:0 substrate and 0.2 mM NADPH. Numerical data with errors are given in Table S4.

2.2. Active Site Mutagenesis of BAMF2522 to Enhance Formation of In-Chain HFAs

An important aim of our study was to diversify the product scope of BAMF2522 in a selective manner, specifically for hydroxylation of in-chain (middle) positions of medium to long-chain fatty acids. Such in-chain preference is scarce among self-sufficient CYPs, which mainly prefer hydroxylation of ω -1, ω -2 and ω -3 positions of their fatty acid substrates [18]. In fact among CYP102 family, the largest group of self-sufficient CYPs, BAMF2522 is the only wild-type enzyme that can catalyze in-chain hydroxylation of palmitic acid from ω -1 up to ω -7 position (hydroxylating all seven positions to some extent) [36]. In addition, we previously observed that a single mutant of BAMF2522 (F89I) was able to shift its regioselectivity more towards in-chain positions, leading to hydroxylation of all positions from ω -1 to ω -9 at various ratios generating a mixture of sub-terminal and in-chain HFAs [36]. We hypothesized that further engineering of BAMF2522 could give us variants that can generate in-chain hydroxylated HFAs selectively as major products; not only from palmitic acid, but also from various other fatty acids, with high potential for various applications.

In earlier literature studies, CYPs were engineered to modulate their selectivity towards various chain-length fatty acids [44–46]. Based on the previous work on BM3 and on the structural analysis of BAMF2522 homology model, we determined hot-spot residues at the active site as well as at distant locations, for site-directed mutagenesis (Figure 3 and Figure S4). In addition to F89, these positions included, A331, I266, N72, M187, V218, M240, S49 and F53. Of these, highly conserved F89, A331 and I266 residues are close (within 4 Å–7 Å) to both the heme group and the fatty acid substrate in BM3 structure (Figure S4 and Table S6), and have been shown to have significant impact on regioselectivity in various studies [18,45,47,48]. In BM3, F87 (residue corresponding to F89 in BAMF2522) is positioned between the heme iron and the terminal end of the substrate [47]. Being the most commonly mutated residue, F87 has been associated with substrate specificity, substrate positioning, regioselectivity, catalytic activity and coupling [3,45–47,49,50]. Similarly, A331 mutations (corresponding to A328 in BM3) have been shown to affect substrate binding, regioselectivity and turnover rates [48]. Residues corresponding to N72, V218, M240 and M187 were shown to alter regioselectivity in a random engineering study carried out for BM3 [47]. Among these four positions, only M187 is close to the active-site (Figure 3). S49 and F53, equivalent to R47 and Y51 respectively in BM3, are at the mouth of the substrate access channel. These two residues are considered responsible for initial docking of fatty acid substrate (from the carboxylate end) and as gate keeper residues to the substrate binding site, presumably controlling substrate specificity [3]. By performing site-directed mutagenesis at a single site or at multiple sites (in various combinations of the selected residues), we generated eight active mutants and screened them towards six saturated fatty acids; lauric acid (dodecanoic acid; C12:0), myristic acid (tetradecanoic acid; C14:0), pentadecanoic acid (C15:0), palmitic acid (C16:0), stearic acid (octadecanoic acid; C18:0), and arachidic acid (eicosanoic acid; C20:0) (Table S5). Products and the remaining substrates of the enzymatic reactions were quantified by GC-FID or GC-MS, and the identification of the product regioisomers were based on analysis of the fragmentation patterns of the trimethylsilyl (TMS) derivatives of HFAs on mass spectra (Figure 4). In selecting the type of amino acids that will be placed at the chosen mutation sites, we also paid attention at increasing selectivity for a single HFA regioisomer product, in addition to shifting regioselectivity to more in-chain, based on earlier studies [36,47]. Since BAMF2522 had no activity towards unsaturated fatty acids as shown previously [36], our substrate screening only included saturated fatty acids.



Figure 3. Homology model of BAMF2522 shown as ribbon diagram (based on structure of BM3 as the template, PDB ID: 1FAG, Chain A). Mutation sites chosen in this study for the engineering of BAMF2522 are shown in magenta. Heme porphyrin is shown in light brown and blue sticks. Representation of the corresponding mutation sites on the crystal structure of BM3 is given in the Supplementary Material (Figure S4).

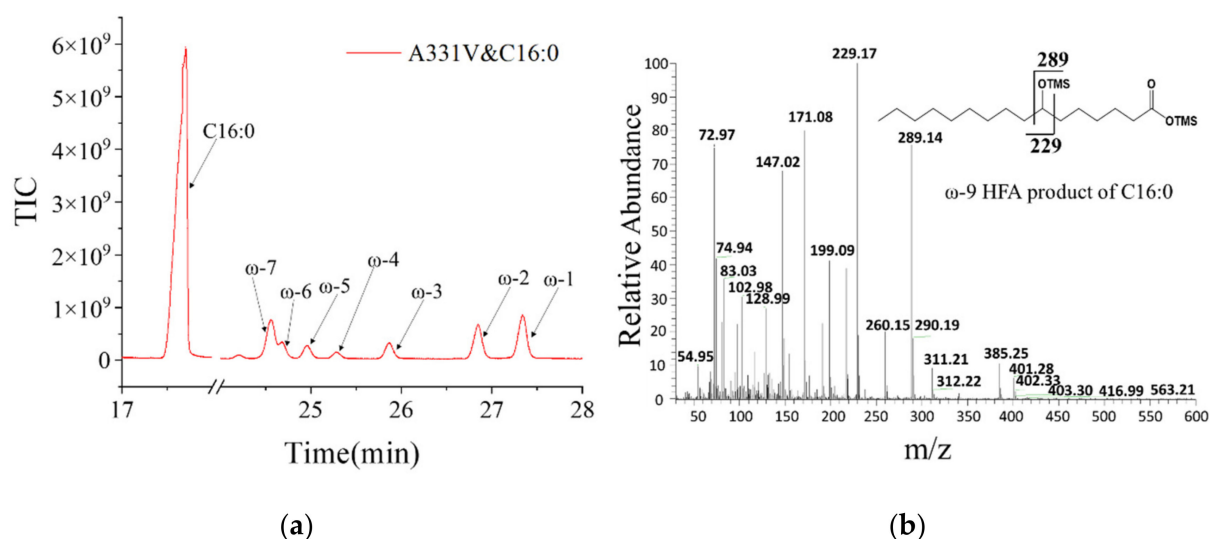


Figure 4. (a) Representative GC chromatogram showing substrate and product peaks from analysis of TMS derivatized reaction extract from conversion of C16:0 substrate by A331V mutant of BAMF2522. (b) Representative mass spectrum for the TMS derivative of ω -9 HFA (7-hydroxy palmitic acid) product of C16:0, indicating the fragmentation pattern used to identify the product. GC chromatograms and mass spectra of all other products are given in the Supplementary Material.

Among the BA2522 mutants tested, F89 single mutants (F89I and F89V), RY5 variant (A331V/F89I/S49R/F53Y), R31 variant (A331V/F89I/N72S/M187T) and R41 variant (A331V/F89I/N72S/M187T/V218A/M240L) exhibited product profiles with high ratios of in-chain HFA products (ω -4 and ω -5 for C12:0; ω -6 and ω -7 for C14:0; ω -8 and ω -9 for C16:0), in comparison to wild-type enzyme and other mutants (Table 1 and Table S5). For example, R41 variant had almost 84% of its total HFA product content as sum of ω -7, ω -8 and ω -9 products, when C16:0 was used as a substrate (Table 1). This ratio was also high for R31 variant, at 77%. Due to poor resolution of the peaks, individual amounts of these in-chain HFA products could not be calculated; however, it was apparent from the GC chromatograms that the majority was the sum of ω -8 and ω -9 products for R31 and R41 variants (Figure S7). Such a shift in regioselectivity is remarkable considered that wild-type BAMF2522 cannot produce any ω -8 or ω -9 products from C16:0, and can produce ω -7 product at only 22% ratio (Table 1). When all mutants and their regioselectivity shifts are compared, mutations at positions of F89, N72 and M187 seemed to have the highest impact. F89, being located between heme and ω -terminus of the substrate (Figure 3), probably affects the substrate alignment with respect to heme group. It is more difficult to address the changes associated with N72S and M187T, since these two residues are positioned at the opposite sides of the carboxylate group of the substrate, but at a pretty long distance (8–10 Å). However, one should keep in mind that the structural judgements here are based on BM3 structure, and even structures of BM3 are not always sufficient to address catalytic or selectivity effects, since a significant reorientation occur during substrate binding and catalysis [47]. Activity and regioselectivity of A331V mutant towards C16:0 was also interesting. Besides exhibiting twice as much activity as wild-type BAMF2522 (29% vs. 14% conversion), A331V mutant generated significantly higher ω -1 product (27% vs. 10% product ratio) than the wild-type enzyme while retaining regioselectivity towards ω -5, ω -6 and ω -7 products. As for C20:0 substrate, A331V was the only active mutant generating five products hydroxylated from ω -1 to ω -5 positions. Only A331 and RY5 variants displayed activity towards C18:0, with equivalent product scope but moderately altered regioselectivity compared to wild-type enzyme, especially towards ω -3 position with RY5 (Table S5). For the assays with C15:0 substrate, it is difficult to assess the extent of regioselectivity shift of the mutants due to an impurity peak that overlapped with ω -2 product peak in whole cell conversions (not present in purified enzyme assays), possibly related to a cell metabolite as described earlier [51]. However, it is apparent that most mutants can generate ω -7 and ω -8 products from C15:0 substrate, although at low levels (ca. 5–10%) (Table S5 and Figure S7). Overall, change in regioselectivity came at the expense of decreased conversion levels in most cases (Table 1 and Table S5), which might partially be due to lower soluble expression levels of the mutants and/or to decreased coupling of NADPH oxidation to substrate hydroxylation. Since our main focus was on regioselectivity, we did not carry out activity optimization for mutants with low total conversions.

Although, none of the BAMF2522 mutants exhibited elevated preference for hydroxylation of a single carbon atom, high overall selectivity for in-chain positions of various fatty acids, especially for ω -8 and ω -9 positions of palmitic acid, was achieved for the first time with a CYP102 enzyme.

Table 1. Total conversion levels and product distribution of BAMF2522 mutants that exhibit highly preferred selectivity for in-chain hydroxylation.

Entry	Subst.	Variant	Total Conv. (%) ¹	Product Distribution (%) ¹								
				ω -9	ω -8	ω -7	ω -6	ω -5	ω -4	ω -3	ω -2	ω -1
1	C12:0	Wild-type	10	-	-	-	-	<2	<2	40	40	17
2	C12:0	F89V	5	-	-	-	-	12	8	49	21	9
3	C12:0	F89I/A331V	4	-	-	-	-	7	13	36	18	27
4	C12:0	RY5 ³	1.2	-	-	-	-	10	14 ± 7	34	15	27 ± 6
5	C12:0	R31 ⁴	3	-	-	-	-	8 ± 2	18	22	40 ± 10	12 ± 5
6	C12:0	R41 ⁵	2	-	-	-	-	18 ± 4	19	36	13	13 ± 3
7	C14:0	Wild-type	28	-	-	<2	<1	2 ± 1	9	46	33	8
8	C14:0	F89V	29 ± 7	-	-	35	10	19	15	12	7	3 ± 1
9	C14:0	F89I	3	-	-	16	12	35	13	13 ± 4	6 ± 2	6
10	C14:0	F89I/A331V	19	-	-	17	6	29	20	10 ± 3	4 ± 2	13
11	C14:0	RY5 ³	4 ± 3	-	-	12	7	28	15 ± 3	14 ± 3	9	16
12	C14:0	R31 ⁴	6	-	-	32 ± 8	12	26	20 ± 5	11 ± 3	<1	<1
13	C14:0	R41 ⁵	9	-	-	36	10 ± 4	30	17	8	<1	<1
14	C16:0	Wild-type	14	-	-	20	9 ± 3	8	10	19	24	10
15	C16:0	F89I	14 ± 3	-	71 ²	-	7	3	2	2	5	9
16	C16:0	A331V	29	-	-	24	9	7	4	9	20	27
17	C16:0	F89I/A331V	8	-	49 ± 2 ²	-	5	3	2	3	9	29
18	C16:0	RY5 ³	10	-	48 ± 1 ²	-	6	4 ± 1	9	7	11	18
19	C16:0	R31 ⁴	5	-	77 ± 2 ²	-	7 ± 1	2 ± 1	2	<2	6	5
20	C16:0	R41 ⁵	7	-	84 ± 1 ²	-	6	2 ± 1	<2	<2	<2	4
21	C20:0	Wild-type	3	-	-	-	-	-	-	49	39	13
22	C20:0	A331V	8 ± 2	-	-	-	-	9 ± 3	11	21	27	31

¹ Both total conversion percentages and product distributions are given as averages of two separate measurements. Standard errors are displayed only for cases where the error is around 20% or over of the mean value, or for significant products. Information on all other mutants and substrates are given in the Supplementary Material (Table S5). ² Due to poor resolution of ω -7, ω -8 and ω -9 HFA product peaks on GC chromatogram, these products are reported as total sum of their percentages. ³ RY5 mutant; A331V/F89I/S49R/F53Y. ⁴ R31 mutant; A331V/F89I/N72S/M187T. ⁵ R41 mutant; A331V/F89I/N72S/M187T/V218A/M240L.

2.3. Site-Saturation Mutagenesis of BAMF2522 to Enhance Selective Formation of In-Chain HFAs with Lauric Acid

In-chain hydroxylated derivatives of lauric acid (C12:0) can be used for synthesis of lactones, which are generated through intramolecular esterification of hydroxy and carboxyl groups of HFA. Such lactones possess various fruity, buttery and oily odors and flavors, which make them valuable molecules with wide uses in fragrance and flavor industry [37,52]. δ -dodecalactone and γ -dodecalactone are the common lauric acid-derived lactones [53]. Although they are naturally formed in fruits and dairy products, their concentrations are generally low [35,52]. Thus, eco-friendly biocatalytic processes for enantioselective synthesis of these valuable lactones from naturally abundant molecules are desired [37]. Whilst HFA derivatives of lauric acid are ideal precursors for lactone synthesis, the presence of the hydroxy group at ω -7 (C5 or δ) and ω -8 (C4 or γ) positions of lauric acid is required for the synthesis of δ -dodecalactone and γ -dodecalactone, respectively. Wild-type BAMF2522 and rational design mutants (described in Section 2.2) were able to generate ω -1 to ω -5 HFAs from lauric acid. Therefore, we hypothesized that semi-rational engineering based on key amino acid residues might render mutants that are able to hydroxylate lauric acid at ω -7 and ω -8 positions. Thus, in order to shift the hydroxylation position more in-chain (towards carboxylate end), we performed site-saturation mutagenesis at residues of A331 and F89. By exchanging each residue separately to all other possible proteinogenic amino acids, we generated a library of 38 single mutants. The activity and selectivity of the library were tested towards lauric acid (Tables 2 and 3). However, no ω -6, ω -7 or ω -8 HFA products were observed. The product scope of the site-saturation mutants was same as the wild-type and the rationally designed mutants described above, exhibiting formation of only ω -1 to ω -5 products. Interestingly, some of the mutants had significantly higher ratio of ω -5 HFA. Specifically, F89P mutant generated ω -5 product at 31% and ω -4 product at 19% of the total products. In addition, ω -5 HFA product was observed at 27% with F89A mutant. Both mutants showed better in-chain selectivity than

the R41 mutant (Tables 1 and 2). Overall, although no new HFA product was obtained with the site-saturation library, there was notable shift in regioselectivity towards in-chain positions with some of the mutants. As a general trend, replacing phenylalanine with smaller residues shifted regioselectivity more towards in-chain positions, consistent with the location of F87 between heme group and terminal chain of the substrate in BM3 structure (see Section 2.2). Further semi-rational engineering and combinatorial mutagenesis approaches can render variants with potential to produce more in-chain HFAs.

Table 2. Total conversion levels and product distribution for the conversion of C12:0 substrate by F89 site-saturation mutants of BAMF2522 (Phenylalanine 89 position was replaced by all other amino acids). Only mutants that exhibited detectable activity are shown.

Entry	Variant	Total Conv. (%) ¹	Product Distribution (%) ¹				
			ω -5	ω -4	ω -3	ω -2	ω -1
1	Wild-type	10	<1	2 ± 1	40	40	17
2	A(Ala)	3	29	15	41	12	2
3	L(Leu)	3 ± 1	<1	4 ± 1	36	45	14
4	I(Ile)	<1	-	-	50	22 ± 7	29
5	V(Val)	5	12	8	49	21	9
6	M(Met)	3	3	3 ± 1	52	31	10
7	P(Pro)	4 ± 1	31	19	38	10	2
8	S(Ser)	4 ± 1	17	11	50	18	5
9	T(Thr)	2	14 ± 3	12 ± 3	48	21	7 ± 2
10	N(Asn)	1	-	-	48	39	13
11	H(His)	6 ± 4	2	2	48	36	12

¹ Both total conversion percentages and product distributions are given as averages of two separate measurements. Standard errors are displayed only for cases where the error is around 20% or over of the mean value, or for significant products.

Table 3. Total conversion levels and product distribution for the conversion of C12:0 substrate by A331 site-saturation mutants of BAMF2522 (Alanine 331 position was replaced by all other amino acids). Only mutants that exhibited detectable activity are shown.

Entry	Variant	Total Conv. (%) ¹	Product Distribution (%) ¹				
			ω -5	ω -4	ω -3	ω -2	ω -1
1	Wild-type	10	<2	2 ± 1	40	40	17
2	G(Gly)	4	-	-	33	38	29
3	I(Ile)	1.4	-	-	25 ± 8	51	25
4	V(Val)	6	-	<2	29	39	30
5	P(Pro)	6	-	-	28	37	35
6	S(Ser)	6	-	-	42	45	14
7	T(Thr)	7	-	-	31	38	31
8	C(Cys)	6	-	-	43	31	26
9	D(Asp)	2	-	-	30	52	18

¹ Both total conversion percentages and product distributions are given as averages of two separate measurements. Standard errors are displayed only for cases where the error is around 20% or over of the mean value, or for significant products.

On another note, for all the assays presented in Sections 2.2 and 2.3, the enzyme was able to function in whole cell form. The advantages of using whole cells is many, including but not limited to; circumventing the need for protein isolation, avoiding supply of expensive NADPH cofactor, higher stability of the enzyme and simplification of the assay procedure.

3. Materials and Methods

3.1. Chemicals

All fatty acids were purchased from Sigma-Aldrich (now Merck, Darmstadt, Germany) in the purest form available (at least 97% purity). 5-aminolevulinic acid (ALA), nicotinamide adenine dinucleotide phosphate (NADPH) and isopropyl-thio- β -D-galactopyranoside (IPTG) were from Roche (Basel, Switzerland). N,O-Bis(trimethylsilyl)trifluoroacetamide with trimethylchlorosilane (BSTFA + TMCS; 99:1) was purchased from Fisher Scientific (Roskilde, Denmark). Unless otherwise noted, all other chemicals are analytical grade and commercially available.

3.2. Site-Directed and Site Saturation Mutagenesis

The gene sequence of BAMF2522 was used as the templates for mutagenesis [36]. Site-directed mutagenesis was performed using QuickChange II mutagenesis kit (Agilent, Santa Clara, CA, USA), following manufacturer's protocol. Genes of the site-saturation mutants were obtained from Sangon Biotech (Shanghai, China). The primers for mutagenesis were obtained from Eurofins Genomics (Ebersberg, Germany) and their sequences are given in the Supplementary Information (Table S1). All mutations were verified by DNA sequencing (Eurofins Genomics) prior to expression and purification.

3.3. Protein Expression and Purification

Plasmids containing wild type or mutated genes were transformed into *E. coli* BL21(DE3) and the transformed cells were cultured in LB medium containing 100 μ g/mL kanamycin at 37 °C. After about 8 h of incubation (at OD 600 ca. 0.6~0.8), the cultures were cooled to 20 °C and induced with 0.5 mM IPTG and supplemented with 0.5 mM ALA (all concentrations final). 1000 \times trace metal mix was also used in expression cultures (1000 \times concentrations: 50 mM FeCl₃, 20 mM CaCl₂, 2 mM NiSO₄, H₃BO₃ 2860 mg, MnCl₂·4H₂O 1810 mg, ZnSO₄·7H₂O 222 mg, Na₂MoO₄·2H₂O 390 mg, CuSO₄·5H₂O 79 mg, Co(NO₃)₂·6H₂O 49 mg). After cultivation of cells for 20 h at 20 °C and 120 rpm, cultures were collected by centrifugation (4000 \times g, 25 min, 4 °C) and the cell pellets were washed twice with 0.85% NaCl. The resulting cell pellets were store at -80 °C until further use.

For purification of wild-type enzymes, cells were resuspended in lysis buffer (Buffer A; 50 mM Tris-HCl, 10 mM imidazole, 200 mM NaCl, pH 7.5; 10 mL buffer/1 g cell). The cell suspensions were disrupted by sonication (10 min sonication time on ice, 3 s on/off cycles, 40% output). The lysate was clarified by centrifugation (11,000 \times g, for 30 min, at 4 °C). The clarified lysate solution was loaded onto a nickel NTA column (5 mL HisTrap HP, GE Healthcare, Uppsala, Sweden) using Äkta Start FPLC system (GE Healthcare). The protein was eluted with buffer B (50 mM Tris-HCl, 300 mM imidazole, 100 mM NaCl, pH 7.5). After fractions containing eluted protein were collected (based on SDS-PAGE analysis, Figure S5), the resulting pool was buffer-exchanged into the storage buffer (50 mM Tris-HCl, 100 mM NaCl, pH 7.5) and concentrated using a 30 kDa molecular weight cut-off centrifugal filter (Amicon Ultra, Darmstadt, Germany). The concentrated protein was aliquoted, flash-frozen with liquid N₂ and stored at -80 °C with 20% (v/v) glycerol until further use. The active protein concentrations were determined by quantifying the amount of heme bound enzyme using pyridine/hemochrome assay following published protocols [54] (Figure S1).

3.4. Activity Assays for Determination of Optimum Conditions

For optimum reaction condition experiments, the typical reaction conditions were as follows; in a final assay volume of 0.5 mL, each reaction contained 0.6 mM substrate (C15:0), 4.0 μ M enzyme, 0.2 mM NADPH and 5% ethanol (all concentrations final). The reactions were quenched with 0.5 mL ethyl acetate, which also acted as the organic phase for extraction of the substrate and product. A final concentration of 20 mM myristic acid was used as the internal standard. Following extraction, derivatization was performed by BSTFA + TMCS (150 μ L, 99:1) and derivatized samples were subjected to GC analysis, as described in the product analysis section.

For determination of optimum temperature, reactions were examined at different temperatures from 4 °C to 70 °C. Assays were run for 15 min in 50 mM Tris-HCl, pH 7.5, with a shaking speed of 500 rpm (Eppendorf Innova 44/44R, Hamburg, Germany) at respective temperatures (following a 30 min pre-incubation period without enzyme to achieve temperature equilibration).

The effect of pH was measured over the pH range 5.0–11.0, using appropriate buffers: acetate-acetic acid for pH 5.0–5.5; NaH₂PO₄-Na₂HPO₄ for pH 6.0–8.0; Tris-HCl for pH 7.1–8.9; MOPS for pH 6.5–8.0; HEPES for pH 7.0–8.0; and Glycine-NaOH for pH 8.6–10.6. The reactions were carried out at 30 °C for 15 min, with a shaking speed of 500 rpm in respective buffers.

Thermostability was determined by measuring the enzyme activity after pre-incubating the enzyme for 60 min at indicated temperatures (4 °C, 20 °C, 30 °C, 40 °C, 50 °C, 60 °C, 70 °C in 50 mM Tris-HCl, pH 7.5). Afterwards, the enzyme was cooled down to 4 °C and the reactions were later carried out at 30 °C and 500 rpm for 15 min.

3.5. Whole Cell Assays for Regioselectivity Analysis

Cell growth and protein expression of wild-type and mutant enzymes were carried out as described above. Expression of the mutant proteins were confirmed by SDS-PAGE analysis of the whole cells (Figure S7). In general, single and double mutants were expressed at good levels (similar levels as the wild-type enzyme), whereas variants with four or more amino acid exchanges exhibited poor expression. Whole cell reactions contained, in a total assay volume of 1 mL (50 mM Tris-HCl, pH 7.5); 100 mg of wet whole cell, 0.5 mg of fatty acid substrate and 5% (v/v) ethanol. Assays were shaken at 220 rpm, 30 °C for 20 h, after which the Bligh-Dyer method was performed for extraction of the lipid substrate and product, as described before [55]. The resulting extract was derivatized with BSTFA + TMCS (99:1) and analyzed by GC-MS or GC-FID for product identification and quantification.

3.6. Product Analysis by GC-FID and GC-MS

GC-FID measurements were performed on a GC-FID (Scion 436-GC, Bruker, Billerica, MA, USA) using a ZB-5HT column (20 m length × 0.18 mm I.D., 0.18 µm film thickness; Phenomenex, Torrance, CA, USA). GC-MS measurements were performed using a Thermo Fisher DSQ II quadrupole mass spectrometer equipped with Trace GC Ultra, TriPlus autosampler and a SPB-1 column (30 m length × 0.25 mm I.D., 0.25 µm film thickness; Sigma, Darmstadt, Germany). For the assays with dodecanoic acid (C12:0), tetradecanoic acid (C14:0) and pentadecanoic acid (C15:0) substrates, total GC running time is 30 min. GC-FID or GC-MS oven temperatures started at 90 °C, held for 1 min, increased initially by 20 °C/min, and later by 2 °C/min up to 220 °C, without holding time. For other substrates, total running GC time is 55 min; GC-FID or GC-MS oven temperatures started at 90 °C, held for 1 min, increased initially by 20 °C/min, later by 2 °C/min up to 220 °C, and held at this temperature for 20 min.

Conversion levels were calculated based on the ratio of the product peak area to the total peak area of both the substrate and the product, as described previously [36]. The percentages of different product regioisomers of the same reaction were calculated based on the peak areas of the respective products compared to total product peak area. For the calculation of peak areas where peaks are poorly resolved, either perpendicular drop method was used or non-overlapping half of the peak was multiplied by 2, in order to obtain peak areas separately for overlapping peaks (assuming a symmetric peak shape, as is the case for most of the peaks observed). The calculation methods depended on resolution and relative intensities of the overlapping peaks. In case of poorly resolved peaks that overlap significantly, total peak areas of multiple products were reported.

3.7. Structural Model

Homology modelling was performed using Modeller 9.21 program [56], as described previously [36]. CYP102A1 BM3 crystal structure (PDB: 1FAG) was used as a template for both enzymes. The structural models were used to confirm the corresponding residues for mutation. UCSF Chimera (developed by the Resource for Biocomputing, Visualization, and Informatics, University of California, San Francisco, with support from NIH P41-GM103311) was used to analyze and prepare structural images [57].

4. Conclusions

In this study, we report optimum temperature and pH conditions as well as thermostability of the enzyme BAMF2522 from *B. amyloliquefaciens* DSM 7, a novel self-sufficient CYP enzyme exhibiting in-chain selectivity for fatty acid hydroxylation. Although BAMF2522 is mostly similar to BM3 and some other studied self-sufficient CYPs, BAMF2522 is able to maintain about 50% of its optimal activity level when assayed at 60 °C for 15 min, thereby showing better performance than wild-type or engineered full-length BM3 enzymes. More importantly, we demonstrated that the hydroxylation position could be further shifted towards in-chain (carboxylate end) by rational and semi-rational protein engineering. We obtained novel BAMF2522 mutants that can achieve product profiles highly enriched with in-chain HFAs. Two mutant variants were able to generate 77% and 84% of their total products as the sum of ω -7, ω -8 and ω -9 HFAs from palmitic acid, a property not seen with other self-sufficient CYPs studied to date in the literature [18,35]. In fact, the only other self-sufficient CYP enzyme that can hydroxylate such in-chain (middle) positions of palmitic acid is a fungal enzyme, CYP505E3, which has been shown to hydroxylate ω -7 position of C12 to C16 fatty acids with high selectivity [35]. Expansion of the product scope by insertion of hydroxy groups at in-chain positions will greatly increase the available repertoire of HFAs for use in materials and cosmetics industry as well as in medical field.

Availability of the enzyme to function in whole cell form, combined with the self-sufficiency of the enzyme, avoid the need for the presence of reductase partners and continuous supply of reducing equivalents, favoring the application potential of the enzyme. Certainly, more studies are required to increase overall conversions and to further characterize promising mutants. Through optimization under process conditions, mutants of BAMF2522 can become ideal for production of HFAs that are enriched in in-chain HFAs. Nevertheless, we believe that studies reported here will greatly assist the efforts for green, sustainable and feasible production of HFAs by enzymatic means for industrial and medical applications.

Supplementary Materials: The following are available online at <https://www.mdpi.com/article/10.3390/catal11060665/s1>, Figure S1: Pyridine hemeochrome difference spectrum of BAMF2522 (A). Spectra are shown for the oxidized (dotted line) and reduced (solid line) forms. Oxidized sample in yellow color and reduced sample in a reddish color (B); Figure S2: Sequence alignment of BM3 and BAMF2522. The mutation positions are highlighted. Sequence alignments were performed by ClustalW; BM3 structure (PDB:1FAG) was used to display the secondary structure and ENDscript website was used for plotting the sequence alignment results (Robert, X. and P. Gouet, Deciphering key features in protein structures with the new ENDscript server. *Nucleic Acids Res*, 2014. 42(Web Server issue): p. W320-4); Figure S3: Structure of wild-type BM3 (pdb id: 1FAG). The residue positions corresponding to mutations performed on BAMF2522 in this study are indicated in magenta color (Table S9). Iron is shown in orange. The residue numbering is according to BM3 sequence; Figure S4: SDS-PAGE analysis the purified BAMF2522 (A), and the color of the protein elution fractions in the collection tube (B). In (A), lane M is protein marker, lane 1 is purified BAMF2522; Figure S5: SDS-PAGE analysis the whole cell protein expression. Lane M: protein marker, Lane1: BAMF2522, Lane2: RY5, Lane3: BAMF2522 I266F, Lane4: BAMF2522 A331V, Lane5: BAMF2522 A331V/F89I, Lane6: BAMF2522 F89I, Lane7: R31, Lane8: R41; Figure S6: Typical GC-MS analysis chromatograms of the derivatized whole-cell oxidation turnovers of BAMF2522 and some variants with dodecanoic, tetradecanoic, pentadecanoic, palmitic, octadecanoic, arachidic and oleic acids; Figure S7: Mass spectra and fragmentation patterns for the HFA products obtained from enzymatic

transformations in this study; Table S1: Primers used for site-directed mutagenesis of BAMF2522, Table S2: Numerical data for temperature dependence experiments, Table S3: Numerical data for pH dependence experiments, Table S4: Numerical data for thermostability measurements, Table S5: Total conversion levels and regioselectivity data for the hydroxylation of different substrates by wild-type and rational design mutants of BAMF2522, Table S6: Comparison of the mutated residue positions in the protein sequences of BM3 and BAMF2522.

Author Contributions: Conceptualization, Y.W., Z.G., R.G. and B.E.E.; funding acquisition, Z.G. and R.G.; investigation, L.Z., Y.Z. and Z.S.; methodology, Y.W., Z.G., R.G. and B.E.E.; supervision, Y.W., Z.G., R.G. and B.E.E.; validation, L.Z., Y.Z. and Z.S.; visualization, L.Z., Y.Z. and Z.S.; writing—original draft, L.Z. and B.E.E.; writing—review and editing, Y.Z., Y.W., Z.G. and R.G. All authors have read and agreed to the published version of the manuscript.

Funding: This work was supported by the Department of Science and Technology of Jilin Province (Grant no. 20170101033JC), by the Novo Nordisk Foundation (grant no. NNF16OC0021740) and by AUFF-NOVA from Aarhus Universitets Forskningsfond (AUFF-E-2015-FLS-9-12).

Data Availability Statement: The data presented in this study are available on request from the corresponding author.

Conflicts of Interest: The authors declare no conflict of interest.

References

1. Groves, J.T. Cytochrome P450 enzymes: Understanding the biochemical hieroglyphs. *F1000Research* **2015**, *4*. [[CrossRef](#)]
2. Guengerich, F.P. Mechanisms of Cytochrome P450-Catalyzed Oxidations. *ACS Catal.* **2018**, *8*, 10964–10976. [[CrossRef](#)] [[PubMed](#)]
3. Whitehouse, C.J.; Bell, S.G.; Wong, L.L. P450(BM3) (CYP102A1): Connecting the dots. *Chem. Soc. Rev.* **2012**, *41*, 1218–1260. [[CrossRef](#)] [[PubMed](#)]
4. Dennig, A.; Kuhn, M.; Tassoti, S.; Thiessenhusen, A.; Gilch, S.; Bulter, T.; Haas, T.; Hall, M.; Faber, K. Oxidative Decarboxylation of Short-Chain Fatty Acids to 1-Alkenes. *Angew. Chem. Int. Ed. Engl.* **2015**, *54*, 8819–8822. [[CrossRef](#)] [[PubMed](#)]
5. Oliw, E.H.; Bylund, J.; Herman, C. Bisallylic hydroxylation and epoxidation of polyunsaturated fatty acids by cytochrome P450. *Lipids* **1996**, *31*, 1003–1021. [[CrossRef](#)] [[PubMed](#)]
6. Ahr, H.; King, L.; Nastainczyk, W.; Ullrich, V. The mechanism of reductive dehalogenation of haloethane by liver cytochrome P450. *Biochem. Pharmacol.* **1982**, *31*, 383–390. [[CrossRef](#)]
7. Rahimtula, A.D.; O'Brien, P.J. Hydroperoxide dependent O-dealkylation reactions catalyzed by liver microsomal cytochrome P450. *Biochem. Biophys. Res. Commun.* **1975**, *62*, 268–275. [[CrossRef](#)]
8. Volz, T.J.; Rock, D.A.; Jones, J.P. Evidence for two different active oxygen species in cytochrome P450 BM3 mediated sulfoxidation and N-dealkylation reactions. *J. Am. Chem. Soc.* **2002**, *124*, 9724–9725. [[CrossRef](#)]
9. Hammer, S.C.; Kubik, G.; Watkins, E.; Huang, S.; Minges, H.; Arnold, F.H. Anti-Markovnikov alkene oxidation by metal-oxo—mediated enzyme catalysis. *Science* **2017**, *358*, 215–218. [[CrossRef](#)]
10. Denisov, I.G. Structure and Chemistry of Cytochrome P450. *Chem. Rev.* **2005**, *105*, 2253–2277. [[CrossRef](#)]
11. Eser, B.E.; Zhang, Y.; Zong, L.; Guo, Z. Self-sufficient Cytochrome P450s and Their Potential Applications in Biotechnology. *Chin. J. Chem. Eng.* **2020**. [[CrossRef](#)]
12. Jung, S.T.; Lauchli, R.; Arnold, F.H. Cytochrome P450: Taming a wild type enzyme. *Curr. Opin. Biotechnol.* **2011**, *22*, 809–817. [[CrossRef](#)]
13. Fasan, R. Tuning P450 Enzymes as Oxidation Catalysts. *ACS Catal.* **2012**, *2*, 647–666. [[CrossRef](#)]
14. Urlacher, V.B.; Girhard, M. Cytochrome P450 Monooxygenases in Biotechnology and Synthetic Biology. *Trends Biotechnol.* **2019**, *37*, 882–897. [[CrossRef](#)]
15. Kaluzna, I.; Schmitges, T.; Straatman, H.; van Tegelen, D.; Müller, M.; Schürmann, M.; Mink, D. Enabling Selective and Sustainable P450 Oxygenation Technology. Production of 4-Hydroxy- α -isophorone on Kilogram Scale. *Org. Process. Res. Dev.* **2016**, *20*, 814–819. [[CrossRef](#)]
16. Pflug, S.; Richter, S.M.; Urlacher, V.B. Development of a fed-batch process for the production of the cytochrome P450 monooxygenase CYP102A1 from *Bacillus megaterium* in *E. coli*. *J. Biotechnol.* **2007**, *129*, 481–488. [[CrossRef](#)]
17. Ciaramella, A.; Minerdi, D.; Gilardi, G. Catalytically self-sufficient cytochromes P450 for green production of fine chemicals. *Rendiconti Lincei* **2016**, *28*, 169–181. [[CrossRef](#)]
18. Hammerer, L.; Winkler, C.K.; Kroutil, W. Regioselective Biocatalytic Hydroxylation of Fatty Acids by Cytochrome P450s. *Catal. Lett.* **2018**, *148*, 787–812. [[CrossRef](#)]
19. Metzger, J.O.; Bornscheuer, U. Lipids as renewable resources: Current state of chemical and biotechnological conversion and diversification. *Appl. Microbiol. Biotechnol.* **2006**, *71*, 13–22. [[CrossRef](#)]
20. Lu, W.; Ness, J.E.; Xie, W.; Zhang, X.; Minshull, J.; Gross, R.A. Biosynthesis of monomers for plastics from renewable oils. *J. Am. Chem. Soc.* **2010**, *132*, 15451–15455. [[CrossRef](#)]

21. Durairaj, P.; Malla, S.; Nadarajan, S.P.; Lee, P.G.; Jung, E.; Park, H.H.; Kim, B.G.; Yun, H. Fungal cytochrome P450 monooxygenases of *Fusarium oxysporum* for the synthesis of omega-hydroxy fatty acids in engineered *Saccharomyces cerevisiae*. *Microb. Cell Fact.* **2015**, *14*, 45. [[CrossRef](#)]
22. Zhang, Y.; Eser, B.E.; Kristensen, P.; Guo, Z. Fatty acid hydratase for value-added biotransformation: A review. *Chin. J. Chem. Eng.* **2020**, *28*, 2051–2063. [[CrossRef](#)]
23. Kim, K.R.; Oh, D.K. Production of hydroxy fatty acids by microbial fatty acid-hydroxylation enzymes. *Biotechnol. Adv.* **2013**, *31*, 1473–1485. [[CrossRef](#)]
24. Ogawa, J. New lipid science in our inner ecosystem. *Eur. J. Lipid Sci. Technol.* **2015**, *117*, 577–578. [[CrossRef](#)]
25. Moraes-Vieira, P.M.; Saghatelian, A.; Kahn, B.B. GLUT4 expression in adipocytes regulates de novo lipogenesis and levels of a novel class of lipids with antidiabetic and anti-inflammatory effects. *Diabetes* **2016**, *65*, 1808–1815. [[CrossRef](#)]
26. Syed, I.; Lee, J.; Peroni, O.D.; Yore, M.M.; Moraes-Vieira, P.M.; Santoro, A.; Wellenstein, K.; Smith, U.; McGraw, T.E.; Saghatelian, A.; et al. Methodological Issues in Studying PAHSA Biology: Masking PAHSA Effects. *Cell Metab.* **2018**, *28*, 543–546. [[CrossRef](#)]
27. Yore, M.M.; Syed, I.; Moraes-Vieira, P.M.; Zhang, T.; Herman, M.A.; Homan, E.A.; Patel, R.T.; Lee, J.; Chen, S.; Peroni, O.D.; et al. Discovery of a class of endogenous mammalian lipids with anti-diabetic and anti-inflammatory effects. *Cell* **2014**, *159*, 318–332. [[CrossRef](#)]
28. Zhou, P.; Santoro, A.; Peroni, O.D.; Nelson, A.T.; Saghatelian, A.; Siegel, D.; Kahn, B.B. PAHSAs enhance hepatic and systemic insulin sensitivity through direct and indirect mechanisms. *J. Clin. Investig.* **2019**, *129*, 4138–4150. [[CrossRef](#)]
29. Serhan, C.N. Pro-resolving lipid mediators are leads for resolution physiology. *Nature* **2014**, *510*, 92–101. [[CrossRef](#)]
30. Fredman, G.; Spite, M. Specialized pro-resolving mediators in cardiovascular diseases. *Mol. Asp. Med.* **2017**, *58*, 65–71. [[CrossRef](#)]
31. Spite, M.; Claria, J.; Serhan, C.N. Resolvins, specialized proresolving lipid mediators, and their potential roles in metabolic diseases. *Cell Metab.* **2014**, *19*, 21–36. [[CrossRef](#)] [[PubMed](#)]
32. Huang, X.; Groves, J.T. Beyond ferryl-mediated hydroxylation: 40 years of the rebound mechanism and C-H activation. *J. Biol. Inorg. Chem.* **2017**, *22*, 185–207. [[CrossRef](#)] [[PubMed](#)]
33. Buerger, M.B.; Dennig, A.; Nidetzky, B. Process intensification for cytochrome P450 BM3-catalyzed oxy-functionalization of dodecanoic acid. *Biotechnol. Bioeng.* **2020**. [[CrossRef](#)] [[PubMed](#)]
34. Lundemo, M.T.; Woodley, J.M. Guidelines for development and implementation of biocatalytic P450 processes. *Appl. Microbiol. Biotechnol.* **2015**, *99*, 2465–2483. [[CrossRef](#)]
35. Maseme, M.J.; Pennec, A.; van Marwijk, J.; Opperman, D.J.; Smit, M.S. CYP505E3: A Novel Self-Sufficient ω -7 In-Chain Hydroxylase. *Angew. Chem. Int. Ed.* **2020**, *59*, 10359–10362. [[CrossRef](#)]
36. Zong, L.; Gao, R.; Guo, Z.; Shao, Z.; Wang, Y.; Eser, B.E. Characterization and modification of two self-sufficient CYP102 family enzymes from *Bacillus amyloliquefaciens* DSM 7 with distinct regioselectivity towards fatty acid hydroxylation. *Biochem. Eng. J.* **2021**, *166*, 107871. [[CrossRef](#)]
37. Manning, J.; Tavanti, M.; Porter, J.L.; Kress, N.; De Visser, S.P.; Turner, N.J.; Flitsch, S.L. Regio- and Enantio-selective Chemo-enzymatic C-H-Lactonization of Decanoic Acid to (S)-delta-Decalactone. *Angew. Chem. Int. Ed. Engl.* **2019**, *58*, 5668–5671. [[CrossRef](#)]
38. Saab-Rincón, G.; Alwaseem, H.; Guzmán-Luna, V.; Olvera, L.; Fasan, R. Stabilization of the Reductase Domain in the Catalytically Self-Sufficient Cytochrome P450BM3 by Consensus-Guided Mutagenesis. *ChemBioChem* **2018**, *19*, 622–632. [[CrossRef](#)]
39. Ruettinger, R.T.; Fulco, A. Epoxidation of unsaturated fatty acids by a soluble cytochrome P-450-dependent system from *Bacillus megaterium*. *J. Biol. Chem.* **1981**, *256*, 5728–5734. [[CrossRef](#)]
40. Fürst, M.J.L.J.; Kerschbaumer, B.; Rinnofner, C.; Migglautsch, A.K.; Winkler, M.; Fraaije, M.W. Exploring the Biocatalytic Potential of a Self-Sufficient Cytochrome P450 from *Thermothelomyces thermophila*. *Adv. Synth. Catal.* **2019**, *361*, 2487–2496. [[CrossRef](#)]
41. Baker, G.J.; Girvan, H.M.; Matthews, S.; McLean, K.J.; Golovanova, M.; Waltham, T.N.; Rigby, S.E.J.; Nelson, D.R.; Blankley, R.T.; Munro, A.W. Expression, Purification, and Biochemical Characterization of the Flavocytochrome P450 CYP505A30 from *Myceliophthora thermophila*. *ACS Omega* **2017**, *2*, 4705–4724. [[CrossRef](#)]
42. Eiben, S.; Bartelmäs, H.; Urlacher, V.B. Construction of a thermostable cytochrome P450 chimera derived from self-sufficient mesophilic parents. *Appl. Microbiol. Biotechnol.* **2007**, *75*, 1055–1061. [[CrossRef](#)]
43. Salazar, O.; Cirino, P.C.; Arnold, F.H. Thermostabilization of a cytochrome P450 peroxygenase. *ChemBioChem* **2003**, *4*, 891–893. [[CrossRef](#)]
44. Zorn, K.; Oroz-Guinea, I.; Brundiek, H.; Bornscheuer, U.T. Engineering and application of enzymes for lipid modification, an update. *Prog. Lipid Res.* **2016**, *63*, 153–164. [[CrossRef](#)]
45. Dietrich, M.; Do, T.A.; Schmid, R.D.; Pleiss, J.; Urlacher, V.B. Altering the regioselectivity of the subterminal fatty acid hydroxylase P450 BM-3 towards gamma- and delta-positions. *J. Biotechnol.* **2009**, *139*, 115–117. [[CrossRef](#)]
46. Cirino, P.C.; Arnold, F.H. Regioselectivity and activity of cytochrome P450 BM-3 and mutant F87A in reactions driven by hydrogen peroxide. *Adv. Synth. Catal.* **2002**, *344*, 932–937. [[CrossRef](#)]
47. Brühlmann, F.; Fourage, L.; Ullmann, C.; Haefliger, O.P.; Jeckelmann, N.; Dubois, C.; Wahler, D. Engineering cytochrome P450 BM3 of *Bacillus megaterium* for terminal oxidation of palmitic acid. *J. Biotechnol.* **2014**, *184*, 17–26. [[CrossRef](#)]

48. Haines, D.C.; Hegde, A.; Chen, B.; Zhao, W.; Bondlela, M.; Humphreys, J.M.; Mullin, D.A.; Tomchick, D.R.; Machius, M.; Peterson, J.A. A Single Active-Site Mutation of P450BM-3 Dramatically Enhances Substrate Binding and Rate of Product Formation. *Biochemistry* **2011**, *50*, 8333–8341. [[CrossRef](#)]
49. Di Nardo, G.; Gilardi, G. Optimization of the bacterial cytochrome P450 BM3 system for the production of human drug metabolites. *Int. J. Mol. Sci.* **2012**, *13*, 15901–15924. [[CrossRef](#)]
50. Seifert, A.; Vomund, S.; Grohmann, K.; Kriening, S.; Urlacher, V.B.; Laschat, S.; Pleiss, J. Rational Design of a Minimal and Highly Enriched CYP102A1 Mutant Library with Improved Regio-, Stereo- and Chemoselectivity. *ChemBioChem* **2009**, *10*, 853–861. [[CrossRef](#)]
51. Munday, S.D.; Maddigan, N.K.; Young, R.J.; Bell, S.G. Characterisation of two self-sufficient CYP102 family monooxygenases from *Ktedonobacter racemifer* DSM44963 which have new fatty acid alcohol product profiles. *Biochim. Biophys. Acta* **2016**, *1860*, 1149–1162. [[CrossRef](#)]
52. Maga, J.A.; Katz, I. Lactones in foods. *Crit. Rev. Food Sci. Nutr.* **1976**, *8*, 1–56. [[CrossRef](#)]
53. An, J.-U.; Oh, D.-K. Increased production of γ -lactones from hydroxy fatty acids by whole *Waltomyces lipofer* cells induced with oleic acid. *Appl. Microbiol. Biotechnol.* **2013**, *97*, 8265–8272. [[CrossRef](#)]
54. Barr, I.; Guo, F. Pyridine Hemochromagen Assay for Determining the Concentration of Heme in Purified Protein Solutions. *Bio-protocol* **2015**, *5*, e1594. [[CrossRef](#)]
55. Eser, B.E.; Poborsky, M.; Dai, R.; Kishino, S.; Ljubic, A.; Takeuchi, M.; Jacobsen, C.; Ogawa, J.; Kristensen, P.; Guo, Z. Rational Engineering of Hydratase from *Lactobacillus acidophilus* Reveals Critical Residues Directing Substrate Specificity and Regioselectivity. *ChemBioChem* **2020**, *21*, 550–563. [[CrossRef](#)] [[PubMed](#)]
56. Webb, B.; Sali, A. Comparative Protein Structure MODELING Using MODELLER. *Curr. Protoc. Bioinform.* **2016**. [[CrossRef](#)] [[PubMed](#)]
57. Pettersen, E.F.; Goddard, T.D.; Huang, C.C.; Couch, G.S.; Greenblatt, D.M.; Meng, E.C.; Ferrin, T.E. UCSF Chimera—Visualization system for exploratory research and analysis. *J. Comput. Chem.* **2004**, *25*, 1605–1612. [[CrossRef](#)] [[PubMed](#)]